Is There a Robust Technique for Selecting Aspect Ratios in Line Charts?

Yunhai Wang, Zeyu Wang, Lifeng Zhu, Jian Zhang, Chi-Wing Fu,
Zhanglin Cheng, Changhe Tu, and Baoquan Chen

Abstract—The aspect ratio of a line chart heavily influences the perception of the underlying data. Different methods explore different criteria in choosing aspect ratios, but so far, it was still unclear how to select aspect ratios appropriately for any given data. This paper provides a guideline for the user to choose aspect ratios for any input 1D curves by conducting an in-depth analysis of aspect ratio selection methods both theoretically and experimentally. By formulating several existing methods as line integrals, we explain their parameterization invariance. Moreover, we derive a new and improved aspect ratio selection method, namely the L_1-LOR (local orientation resolution), with a certain degree of parameterization invariance. Furthermore, we connect different methods, including AL (arc length based method), the banking to 45° principle, RV (resultant vector) and AS (average absolute slope), as well as L_1-LOR and AO (average absolute orientation). We verify these connections by a comparative evaluation involving various data sets, and show that the selections by RV and L_1-LOR are complementary to each other for most data. Accordingly, we propose the dual-scale banking technique that combines the strengths of RV and L_1-LOR, and demonstrate its practicability using multiple real-world data sets.

Index Terms—Aspect ratio, parameterization invariance, line integral, banking to 45°, orientation resolution.

1 Introduction

Line charts are commonly used for visualizing time series such as stock market values, population statistics, and scientific data. By plotting values over time, trends in the data can be revealed by the slopes of the line segments. However, the aspect ratio of the plot, i.e., height to width ratio, would influence the orientations of the line segments, thus affecting the visual perception of the trends [1]. Choosing an appropriate aspect ratio is therefore highly essential for a fair presentation of the data trend. Fig. 1 shows an example using different aspect ratios to plot the same data, where a small aspect ratio (Fig. 1(a)) highlights the steeper increase around 1983 and then a gradual decrease until 1990, while a large aspect ratio (Fig. 1(b)) emphasizes more on the fast oscillations over time.

Cleveland et al. [3] pioneered the principle of *banking to* 45°, which laid the perceptual foundation for selecting the aspect ratio. Based on the observation that the discriminability of adjacent line segments can be maximized when the average orientation of all the line segments is 45°, Cleveland et al. [4], [5], [6] proposed three methods for aspect ratio selection: *median slope* (MS), *average absolute orientation* (AO), and *arc length weighted average absolute orientation* (AWO), where AWO yields reasonable aspect ratios in general. To further improve the visual perception, Heer and Agrawala [7] directly maximize the range of the orientations spanned by the line segments (which is usually denoted as the orientation resolution) using two alternative methods: *global orientation resolution* (GOR) and *local orientation resolution* (LOR), where the orientation resolution is defined as the range of orientation spanned by the segments.

Taking other directions to approach the problem, Guha and Cleveland [8] and Talbot et al. [9] independently developed the *resultant vector* (RV) and *arc length based* (AL) methods, which are derived from the plot's "resultant vector" and the curve's arc length, respectively. Talbot et al. [9] showed several advantages of AL and RV over previous methods, among which the property of parameterization invariance is especially important, since it guarantees that the method would generate the same aspect ratio for the same given curve regardless of how we parameterize the curve into line segments. Namely, AL and RV are both invariant

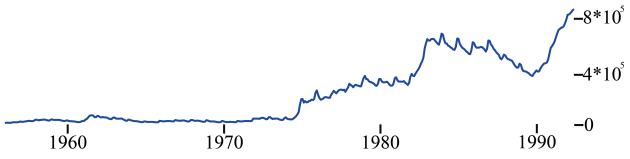

(a) Aspect ratio = 0.236

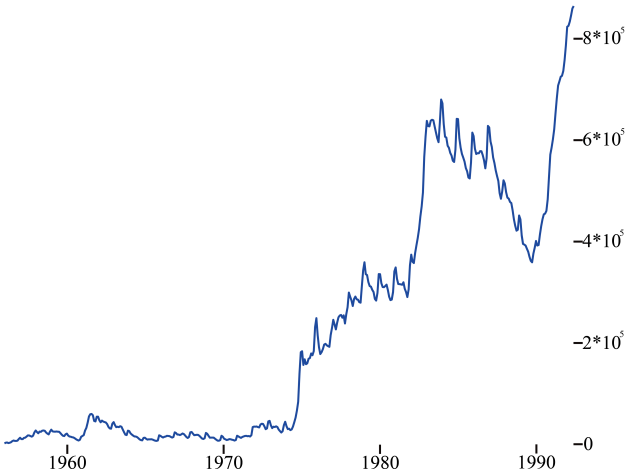

(b) Aspect ratio = 0.752

Fig. 1 Illustrating how the aspect ratio affects the graphical perception of trends using the *dole* dataset [2], which shows the numbers of persons receiving unemployment benefits in Australia from Jan. 1956 to Jul. 1992.

- *Y. Wang, Z. Wang, C. Tu, and B. Chen are with Shandong University E-mail: see cloudseawang@gmail.com*
- *L. Zhu is with Southeast University*
- *J. Zhang is with CNIC, CAS.*
- *C.-W. Fu is with the Chinese University of Hong Kong and VRHIT SIAT.*
- *Z. Cheng and Z. Wang are with VCC SIAT, CAS.*

TABLE 1 Full names, abbreviations, references, definitions, and the properties of parameterization invariance of important aspect ratio selection methods, which are classified into four categories indicated by separator lines in terms of the banking heuristics: average absolute slope/orientation, orientation resolution, resultant vector, and arc length, respectively.

Name of Method	Abbr.	Ref.	Def.	Para. Invar.
Median Absolute **S**lope	MS	[3]	Eq. 3	×
Average Absolute **S**lope	AS	[7]	Eq. 4	×
Average Absolute **O**rientation	AO	[3]	Eq. 5	×
Arc Length **W**eighted Average Absolute **O**rientation	AWO	[4]	Eq. 6	✓
Global **O**rientation **R**esolution	GOR	[7]	Eq. 8	×
Local **O**rientation **R**esolution	LOR	[7]	Eq. 9	×
$\boldsymbol{L_1}$-norm based **L**ocal **O**rientation **R**esolution	L_1-LOR	Ours	Eq. 17	✓
Resultant **V**ector	RV	[8]	Eq. 10	✓
Arc **L**ength	AL	[9]	Eq. 11	✓

under changes to the sampling of the data over time in a regular or irregular way. However, it is still not yet clear why they have such a property, and whether there is any connection between AL, RV and the principle of banking to 45° [3].

In our previous work [10], we introduced the line integral to study the parameterization invariance of AL and RV, and connect them with the principle of banking to 45°. Nonetheless, we only explored the mathematical foundation of AL method and quantitatively evaluated a subset of existing aspect ratio selection methods. In this work, we present an in-depth study of several different aspect ratio selection methods both theoretically and experimentally. By then, we provide guidelines for the user to choose aspect ratio selection method for any input data. This is achieved with four new contributions.

- First, we derived a new aspect ratio selection method, namely L_1-LOR (local orientation resolution), which is parameterization invariant for monotonic data.
- Second, we established the connection between banking to 45° and maximization of orientation resolution by finding an appropriate condition that L_1-LOR performs similarly to AO.
- Third, we conducted a comprehensive evaluation extensively on various aspect ratio selection methods, see Table 1. Results show that both RV and L_1-LOR are robust to noise and outlier, and their selected aspect ratios are complementary, i.e., revealing different patterns of interest for most data.
- Lastly, we proposed the dual-scale banking technique that combines the strength of RV and L_1-LOR, and presented case studies to demonstrate its practicability with multiple data.

The remainder of the paper is divided into six sections. After reviewing previous works in Section 2, we describe how to formulate various existing methods as line integrals in Section 3 and derive the theoretical connections between different methods in Section 4. Then, we study the comparative evaluation results of various methods in Section 5, and propose the dual-scale banking technique in Section 6. Finally, we conclude the paper by discussing the need for perceptual criteria in Section 7.

2 Related Work

Cleveland et al. [3], [4], [5] systematically studied how the aspect ratio affects the judgement of slope ratios, and developed several methods for choosing proper aspect ratios. Later, more methods [7], [8], [9], [11] were developed for simple and robust aspect ratio selection. Before reviewing various methods in Section 2.3, we briefly summarize their perceptual foundation below.

2.1 Empirical Studies

Cleveland et al. [3] hypothesized that the accuracy of slope ratio judgements increases with *orientation resolution*, and conducted various human-subject experiments for verifying it. By fitting an empirical model to the experimental results, they showed that the judgement error is minimized when line segments are centered around 45°. This is the banking to 45° principle. This experiment, however, only tested limited variations of slope ratios, so Talbot et al. [12] further expanded the experimental design and developed an empirical model that provides strong evidence that slope ratio estimation errors are *not* minimized around 45°. As far as we know, there are only two such studies in the field of perception for slope ratio judgement, although many researchers studied the influence of aspect ratios on the perception of 2D elements such as graph shapes [13], areas [14], [15], and correlations [16], [17].

2.2 Perceptual Arguments

Cleveland et al. [3] showed that the accuracy of slope judgement is best when the *orientation resolution* is maximized, and such a condition is equivalent to centering the absolute value of the *midangle* (average orientation) at 45°. These two arguments are the foundation of most aspect ratio selection methods.

Suppose s_1 and s_2 are the slopes of two line segments in the data space, s.t. $s_1 > s_2 > 0$. For a given aspect ratio α of the display, their corresponding slopes in the plot are αs_1 and αs_2, and the orientation resolution $\gamma(\alpha)$ is $|\arctan(\alpha s_1) - \arctan(\alpha s_2)|$, while the midangle $m(\alpha)$ is $\big(\arctan(\alpha s_1) + \arctan(\alpha s_2)\big)/2$. Let $f{=}s_2/s_1$ and $\lambda{=}\alpha\sqrt{s_1 s_2}$, we can rewrite αs_1 and αs_2 as $\lambda/\sqrt{f}$ and $\lambda\sqrt{f}$, respectively, and rewrite $\gamma(\alpha)$ and $m(\alpha)$ as

$$\gamma(\alpha) = |\arctan(\lambda/\sqrt{f}) - \arctan(\lambda\sqrt{f})| \text{ , and} \quad (1)$$

$$m(\alpha) = \frac{1}{2}\big(\arctan(\lambda/\sqrt{f}) + \arctan(\lambda\sqrt{f})\big) \text{ , resp.} \quad (2)$$

For $\lambda = 1$, the orientation resolution $\gamma(\alpha)$ reaches its maximum of $90° - 2\arctan(\sqrt{f})$ when the midangle $m(\alpha)$ is 45°. This also holds for line segments with negative slopes with $m(\alpha) = -45°$. However, there are many line segments in a line chart, and the slopes of some line segment pairs may have different signs. It is unclear whether the equivalence still holds for such cases.

2.3 Aspect Ratio Selection Methods

Based on the above criteria, Cleveland et al. and other researchers developed various methods for aspect ratio selection. As listed in Table 1, these methods can be classified into four categories: the first two categories are based on a generalization of *midangle* and *orientation resolution*, while the other two do not directly follow the perceptual hypotheses presented in Section 2.1.

To compare between methods, we consider a data set with n connecting line segments. First, we follow [7] to normalize the data, so that the data bounding rectangle becomes a square. Then, we denote Δx_i and Δy_i as the displacements of the i-th line segment in x and y directions, respectively, and $s_i = \Delta y_i/\Delta x_i$ as its slope.

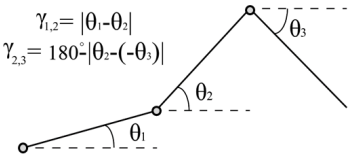

Fig. 2 Illustrating the concept of orientation resolution, which is defined as the smallest acute angle between a pair of line segments.

MS, AS, AO, and AWO belong to the same category of methods that aims to bank the line segments to 45°. MS and AS work on slopes, while AO and AWO work on orientations (line segment angles). In detail, MS uses the reciprocal of the median absolute slope as the key factor for selecting the aspect ratio (α), i.e.,

$$\alpha = 1/\text{median}(\ |s_1|,\ |s_2|,\ ...,\ |s_n|\ )\ , \tag{3}$$

while AS uses the mean absolute slope of the line segments, i.e.,

$$\alpha = 1/\text{mean}(\ |s_1|,\ |s_2|,\ ...,\ |s_n|\ )\ . \tag{4}$$

Comparing with MS and AS, AO chooses the aspect ratio that banks the average absolute orientations to 45° by using an iterative procedure to solve the following optimization:

$$\min_{\alpha\in(0,\infty)}\ |\ \frac{\sum_i |\theta_i(\alpha)|}{n} - 45^\circ\ |\ , \tag{5}$$

where $\theta_i(\alpha)$ is the orientation of the i-th line segment when plotted with the selected aspect ratio (α). However, all three methods generate different results for the same curve represented, or parameterized, with different collections of line segments; see Fig. 3(a) for an example. To address this parameterization invariance issue, AWO weights θ_i by the line segment lengths (l_i):

$$\min_{\alpha\in(0,\infty)}\ |\ \frac{\sum_i |\theta_i(\alpha)| l_i(\alpha)}{\sum_i l_i(\alpha)} - 45^\circ\ |\ . \tag{6}$$

The authors found that AWO works well for most data, and assumed that it is parameterization invariant without providing further explanation on the property.

GOR and LOR. Rather than indirectly maximizing the *orientation resolution* by banking line segments to 45°, Heer and Agrawala [7] proposed the *global orientation resolution* (GOR) method that directly maximizes the orientation resolution. First, they define function γ to measure the orientation difference between line segments (see Fig. 2 for illustrations):

$$\gamma_{i,j}\ =\ \min(\ |\theta_i - \theta_j|\ ,\ 180^\circ - |\theta_i - \theta_j|\ )\ . \tag{7}$$

Since $\theta_i \in [-90^\circ, 90^\circ]$, $\gamma_{i,j} \in [0^\circ, 90^\circ]$; GOR finds the aspect ratio that maximizes the sum of $\gamma_{i,j}^2$ over all pairs of line segments:

$$\max_{a\in(0,\infty)} \sum_i \sum_j \gamma_{i,j}^2\ . \tag{8}$$

In practice, GOR usually produces results similar to AO but is more expensive. Hence, *local orientation resolution* (LOR) simplifies Eq. 8 and considers only successive line segment pairs:

$$\max_{a\in(0,\infty)} \sum_{i=1}^{n-1} \gamma_{i,i+1}^2\ . \tag{9}$$

Both methods, however, cannot handle horizontal and vertical line segments, and they are not parameterization invariant. Apparently, their effects are equivalent to centering the orientations of a pair of adjacent line segments at 45°; however, it is not yet clear whether the equivalence still holds for general line charts with multiple line segments. We will show that LOR can be extended to have certain parameterization invariance in Section 3.3 and provide the condition for the equivalence for general line charts in Section 4.3.

RV. Rather than maximizing the orientation resolution, Guha and Cleveland [8] proposed the *resultant vector* (RV) method that banks the line segments using a simple tractable algebraic form:

$$\alpha = \frac{\sum_i |\Delta x_i|}{\sum_i |\Delta y_i|}\ . \tag{10}$$

Geometrically, RV transforms all line segments into the first quadrant (due to the absolute values), and then selects the aspect ratio, such that the slope of the resultant vector equals one. Although RV produces nice results, its perceptual foundation is not clear. In our previous work [10], we proved that RV is a generalization of AS to a continuous representation, and found that it performs similarly to AL but is faster and more stable. In this work, we further show that RV is capable of handling data with redundancy (see Section 5.2), where all the previous methods fail.

AL. Like RV, the *arc length based aspect ratio selection* method (AL) [9] is also *not* derived based on the banking to 45° principle. Rather, AL chooses the aspect ratio that minimizes the total arc length of line segments in the plot while preserving the area of the data bounding box in the plot (see [9] for details):

$$\min_{\alpha\in(0,\infty)} \sum_{i=1}^{n} ||\frac{\Delta x_i}{\sqrt{\alpha}}, \sqrt{\alpha}\Delta y_i||. \tag{11}$$

Here, dividing Δx_i by $\sqrt{\alpha}$ and multiplying Δy_i with $\sqrt{\alpha}$ keep the data bounding box area and $||\cdot||$ is the Euclidean norm.

AL shows many empirical advantages over previous methods. Among them, Talbot et al. [9] found that AL and AWO are parameterization invariant, but not other existing methods. By taking line segments in 2D contour plots as inputs, they compared a subset of previous methods in selecting aspect ratios for 2D contour plots and showed that AL also works well because of its parameterization invariance. However, they did not explain why AL has such a property, and whether there is any connection between this property and the banking to 45° principle. Our previous work [10] explained why AL is parameterization invariant and connected AL with the banking to 45° principle. In this work, we further provide the empirical result in Section 5.1 to strengthen the connection. On the other hand, Talbot et al. [9] suggested to use AL as the default method to select the aspect ratio, however, they did not conduct a comprehensive comparison for all aspect ratio selection methods. In this work, we provide both theoretical analysis and comparison experiments as well as guidelines for users to choose aspect ratio selection methods. Specifically, we found that RV and L_1-LOR both select reasonable aspect ratios for most data but reveal patterns of interest that are complementary.

3 Formulation using Line Integrals

In this section, we describe how to formulate various aspect ratio selection methods as line integrals for explaining their parameterization invariance [10], and then extend LOR to achieve certain parameterization invariance.

3.1 Parameterization Invariant Methods

Given a scalar function $f : C \subset R^n \to R$, where C is a curve, the line integral [18] along C is defined as:

$$\int_C f ds\ =\ \int_a^b f(\mathbf{r}(t))|\mathbf{r}'(t)|dt\ , \tag{12}$$

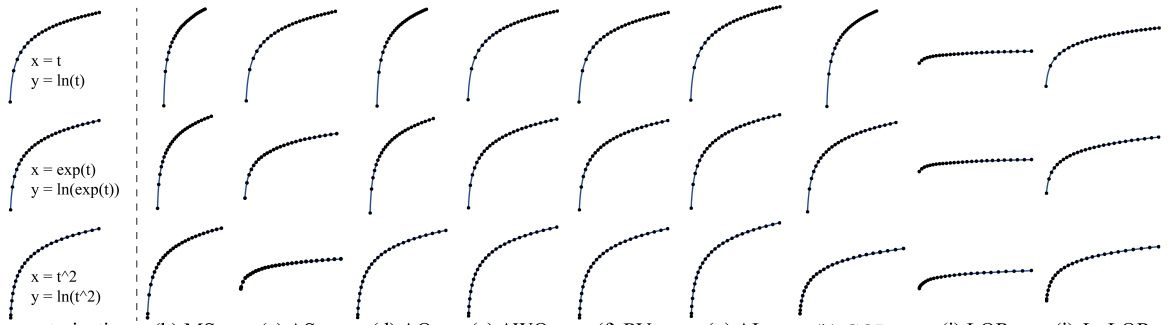

Methods	Means ± std
MS	1.767 ± 0.419
AS	0.685 ± 0.264
AO	1.465 ± 0.434
AWO	0.995 ± 0.001
RV	1 ± 0
AL	1.044 ± 0.004
GOR	0.895 ± 0.206
LOR	0.129 ± 0.068
L_1-LOR	0.515 ± 0.008

(a) Parameterizations (b) MS (c) AS (d) AO (e) AWO (f) RV (g) AL (h) GOR (i) LOR (j) L_1-LOR (k) Aspect ratios

Fig. 3 Comparing various aspect ratio selection methods (including ours (j)) on how they select aspect ratios (b-j) for the same curve "$y = \ln x$" parameterized into line segments in three different ways (a). Results in (b-j) show that the three plots generated by methods AWO, RV, AL and L_1-LOR are almost the same, thus revealing their parameterization invariance. The standard deviations of the aspect ratios selected by various methods are shown in (k): AL, AWO, RV and L_1-LOR have small standard deviations, but not others.

where f is the integrand, ds is the arc length element, and C is parameterized by function $\mathbf{r}(t)$ for $a \le t \le b$ with derivative $\mathbf{r}'(t)$. Note that $\mathbf{r} : [a,b] \to C$ is a bijective parameterization, such that $\mathbf{r}(a)$ and $\mathbf{r}(b)$ are the endpoints of C, and the value of the integral is independent of the parameterization $\mathbf{r}$. A typical application example of line integrals is computing the mass of a wire described by a curve C with a density function f. No matter what $\mathbf{r}$ we used to parameterize C, the total mass is always the same.

Fig. 3(a) shows a curve parameterized in three different ways. If a method is parameterization invariant, the selected aspect ratio should be the same regardless of the parameterization. Below, we represent AL, AWO and RV in line integral forms, and show that they are parameterization invariant; note that the parameterization invariance of RV has not been shown so far.

AL. Since the arc length is inherently a variable of the line integral, Eq. (11) can be represented as follows:

$$\min_{\alpha\in(0,\infty)} \sum_{i=1}^{n} \frac{1}{\sqrt{\alpha}} ||\Delta x_i, \alpha \Delta y_i|| \;=\; \min_{\alpha\in(0,\infty)} \int_C \frac{1}{\sqrt{\alpha}} ds \;, \qquad (13)$$

where the integrand is a constant. Since the arc length ds depends on α, a larger α may not result in a smaller objective. On the other hand, the integral representation provides an alternative to interpret AL. That is, finding the largest squared root of the aspect ratio that produces the shortest arc length. This indicates that AL does not need an explicit area-preserving constraint, and we do not need to simultaneously scale x and y dimensions as done in Eq. (11).

AWO. We can represent AWO using the following line integral:

$$\min_{\alpha\in(0,\infty)} \Big| \frac{\sum_i |\theta_i(\alpha)| l_i(\alpha)}{\sum_i l_i(\alpha)} - 45^\circ \Big| \;=\; \min_{\alpha\in(0,\infty)} \Big| \frac{\int_C |\theta(\alpha,s)| ds}{\int_C ds} - 45^\circ \Big| \;, \qquad (14)$$

where the line orientation $\theta(\alpha,s)$ is a function of the aspect ratio α varying along the arc length s. We can see that integrands (see Eq. (12)) in the numerator and denominator of Eq. (14) are $|\theta(\alpha,s)|$ and one, respectively.

RV. The above line integral representations show that AL and AWO are invariant to parameterization changes. Here, we show that RV also has this property by putting it in a line integral form:

$$\alpha = \frac{\sum_i |\Delta x_i|}{\sum_i |\Delta y_i|} = \frac{\int_C |\cos(\theta(\alpha_0,s))| ds}{\int_C |\sin(\theta(\alpha_0,s))| ds}, \qquad (15)$$

where α_0 is 1 as generated by the data normalization; see [8] for details, and the integrands in the numerator and denominator are $|\cos(\theta(\alpha_0,s))|$ and $|\sin(\theta(\alpha_0,s))|$, respectively. Since RV has a closed form, it can be computed faster than AWO and AL.

In summary, AL, AWO and RV can be represented in line integral forms, so they can select almost the same aspect ratio for the same curve in different parameterizations. See also Fig. 3(k), which shows that the aspect ratios selected by AL, AWO and RV for different parameterizations have very tiny standard deviations. Lastly, note also that the parameterization function $\mathbf{r}$ can be an arbitrary bijective function that need not be an analytic function.

3.2 Parameterization Variant Methods

The line integral representation is a sufficient condition for parameterization invariance [18]. Through extensive experiments, Talbot et al. [9] observed that MS, AS, AO, GOR and LOR are *not* parameterization invariant. See again the examples shown in Fig. 3, the standard deviations of the aspect ratios selected by these methods are significantly far from zeros. Below, we discuss which factors put down the property of parameterization invariance.

MS, AS and AO select the aspect ratio based on the median absolute slope, average absolute slope, and average absolute orientation. Since the computation of median and average values ignore the lengths of the line segments, these methods are sensitive to the parameterization. In contrast, AWO weights the absolute orientations with the lengths of the line segment, so it becomes parameterization invariant. Later in Section 4.2, we will derive and show that RV is a parameterization invariant form of AS.

GOR and LOR select the aspect ratio based on an L_2 norm of $\gamma_{i,j}$. Since $\theta_i \in [-90^\circ, 90^\circ]$, we can rewrite Eq. (7) as

$$\gamma_{i,j} = \begin{cases} |\theta_i - \theta_j| & \text{if } |\theta_i - \theta_j| < 90^\circ \;, \\ 180^\circ - |\theta_i - \theta_j| & \text{otherwise.} \end{cases} \qquad (16)$$

The sub-function for computing $\gamma_{i,j}$ is determined by the difference between $|\theta_i - \theta_j|$ and 90°. Since the parameterization does not take this difference into account, the selected aspect ratio may fluctuate for different parameterizations.

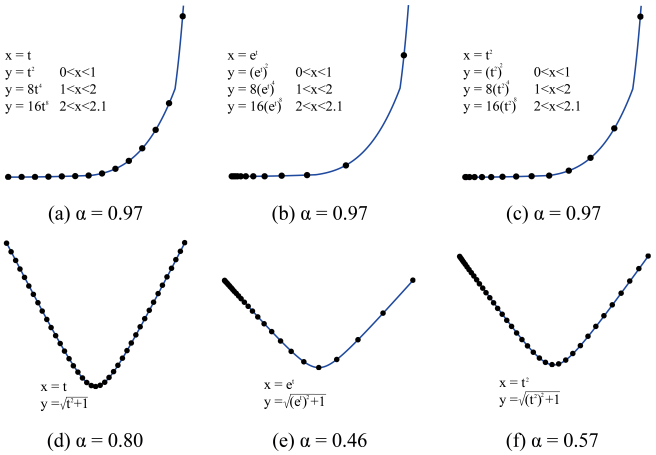

(a) α = 0.97 (b) α = 0.97 (c) α = 0.97

(d) α = 0.80 (e) α = 0.46 (f) α = 0.57

Fig. 4 L_1-LOR is parameterization invariant for monotonous functions (a,b,c), and it exhibits certain variance for curves that have orientation changes (d,e,f).

3.3 L_1-LOR with Certain Parameterization Invariance

We propose a new aspect ratio selection method called L_1-LOR, which has certain parameterization invariance. To create L_1-LOR, we replace the L_2 norm in Eq. (9) with an L_1 norm:

$$\max_{a\in(0,\infty)} \sum_{i=1}^{n-1} \gamma_{i,i+1} = \max_{a\in(0,\infty)} \sum_{i=1}^{n-1} \min(|\theta_{i+1}-\theta_i|, 180^\circ - |\theta_{i+1}-\theta_i|) = \max_{a\in(0,\infty)} \int_C \frac{\min(|\theta_{i+1}-\theta_i|, 180^\circ - |\theta_{i+1}-\theta_i|)}{ds} ds. \tag{17}$$

When $\theta(\alpha, s)$ is a monotonically increasing function, θ_i and θ_{i+1} are both positive, and therefore $\gamma_{i,i+1}$ is always $\theta_{i+1}-\theta_i$. Hence, Eq. (17) can be expressed using the total change in orientations:

$$\max_{a\in(0,\infty)} \sum_{i=1}^{n-1} \gamma_{i,i+1} = \max_{a\in(0,\infty)} \int_C \frac{\theta_{i+1}-\theta_i}{ds} ds, \tag{18}$$

where the sum is $\theta_n - \theta_1$. Likewise, the sum is $\theta_1 - \theta_n$ if $\theta(\alpha, s)$ is monotonic decreasing. The total orientation resolution in these cases only depends on the starting and ending slope of the curve, so L_1-LOR is parameterization invariant in these cases.

The example shown in Fig. 3 is a monotonically increasing function, so the aspect ratios selected by Eq. (18) over the three different parameterizations have little variance. In contrast, LOR does not have the parameterization invariance property (see Fig. 3(h)), due to the L_2 norm. Fig. 4 shows more examples. As long as the plotted curve is monotonic, L_1-LOR is parameterization invariant; see Figs. 4(a,b,c). When the curve is not monotonic, θ_i and θ_{i+1} could have different signs, so $\gamma_{i,i+1}$ is computed by $180^\circ - |\theta_{i+1}-\theta_i|$ (see Eq. (16)), which has different cases depending on the sign of $\theta_{i+1}-\theta_i$. Hence, Eq. (17) is no longer parameterization invariant; see Figs 4(d,e,f).

While parameterization invariance is a desirable property, all methods discussed in Sections 3.2 and 3.3 do not possess this property, but still, they have their own advantages; see Section 5. It is therefore important to obtain guidelines as to which parameterizations will yield reliable results.

4 Connection between Methods

The line integral representation enables us to explore the parameterization invariance of various methods and to group them into parameterization invariance (AWO, AL, RV and L_1-LOR) and parameterization variance (MS, AS, AO, LOR and GOR) methods. Besides parameterization invariance, we may consider perceptual arguments: AWO, AO, AS and MS belong to the group based on the banking to 45° principle, while LOR, GOR and L_1-LOR belong to the group that maximizes the orientation resolution. In contrast, both AL and RV lack perceptual arguments as in other methods, although they are parameterization invariant.

In this section, we explore and derive the connections between various methods, including AL and the banking to 45° principle, RV and AS, as well as L_1-LOR and AO. These are new findings that have not been studied and derived in any previous work.

4.1 Connecting AL and Banking to 45°

Considering only a single line segment, Eq. (11) becomes

$$\min_{\alpha\in(0,\infty)} \sqrt{(\Delta x_i/\sqrt{\alpha})^2 + (\sqrt{\alpha}\Delta y_i)^2}\ ,$$

which attains its minima $\sqrt{2\Delta x_i \Delta y_i}$ when $\alpha = \Delta x_i/\Delta y_i$, or the line orientation = 45°. This indicates that AL also banks a line segment to 45° by enforcing the triangle associated with the line segment to be an isosceles right triangle; see the inset figure.

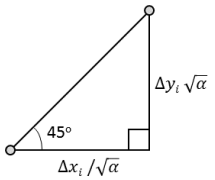

For a curve with multiple line segments, we consider the case that the data points are equally spaced along the X dimension. Hence, we can rewrite Eq. (11) as

$$\min_{\alpha\in(0,\infty)} \frac{\sum_{i=1}^{n}\sqrt{1+\alpha^2|s_i|^2}}{\sqrt{\alpha}}\Delta x_i\ , \tag{19}$$

where s_i is the slope of the i-th line segment. Since a larger $|s_i|$ means a larger arc length, the optimization would then bank the line segments with larger $|s_i|$ to 45° more aggressively. However, it is not clear whether the aspect ratio produced by Eq. (13) for a curve with multiple line segments really converges to a value of *one*. Hence, we propose to compute the bounds of the average absolute slopes generated by AL, and use these bounds to show that AL tends to satisfy the banking to 45° principle.

Bounds of the Average Absolute Slope. Differentiating Eq. (19) with respect to α and setting the derivative to zero, we have

$$\sum_{i=1}^{n} \frac{\alpha^2 s_i^2 - 1}{\sqrt{\alpha^2 s_i^2 + 1}} = 0\ , \tag{20}$$

which can be rewritten as

$$\sum_{i=1}^{n} \frac{(\alpha|s_i|-1)(\alpha|s_i|+1)}{\sqrt{(\alpha|s_i|)^2+1}} = 0\ . \tag{21}$$

Since $\alpha|s_i|$ is always non-negative, we can define ω_i as:

$$\omega_i = \frac{\alpha|s_i|+1}{\sqrt{(\alpha|s_i|)^2+1}}\ , \tag{22}$$

and compute its bounds:

$$1 \le \omega_i = \frac{\alpha|s_i|+1}{\sqrt{(\alpha|s_i|)^2+1}} = \sqrt{1+\frac{2\alpha|s_i|}{\alpha^2 s_i^2+1}} \le \sqrt{1+\frac{2\alpha|s_i|}{2\alpha|s_i|}} = \sqrt{2}\ .$$

where ω_i reaches its minima of 1 when $\alpha|s_i|$=0, and its maxima of $\sqrt{2}$ when $\alpha|s_i|$=1. Putting ω_i into Eq. (21), we get

$$\sum_{i=1}^{n} (\alpha|s_i|-1)\omega_i = 0\ , \tag{23}$$

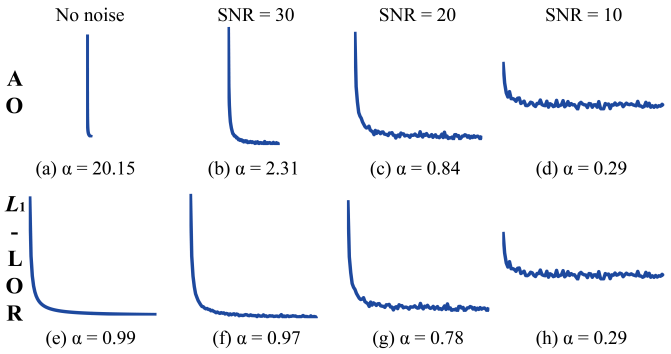

Fig. 5 We add increasing amount of white noise (left to right) to input curve $y = 1/x$; SNR means Signal-to-Noise Ratio. Top and bottom rows are plots produced by AO and L_1-LOR, respectively. When the noise level is high (rightmost plots), AO and L_1-LOR converge and produce plots with a similar aspect ratio.

where α is undefined if $s_i = 0\ \forall i$; otherwise, we can re-arrange the terms in Eq. (23) and obtain

$$\alpha = \frac{\sum_i \omega_i}{\sum_i \omega_i |s_i|}. \tag{24}$$

Multiplying both sides of Eq. (24) with $\sum_i |s_i|/n$ we get

$$\frac{\alpha \sum_i |s_i|}{n} = \frac{\sum_i \omega_i \sum_i |s_i|}{n \sum_i \omega_i |s_i|}, \tag{25}$$

where the left side is the average absolute slope. Since $\omega_i \in [1, \sqrt{2}]$, Eq. (25) attains its minimum when setting all ω_i in its numerator to be 1 and all ω_i in its denominator to $\sqrt{2}$. Likewise, Eq. (25) attains its maximum by setting ω_i in the other way around. Thus, the range of the average absolute slope is $[\sqrt{2}/2, \sqrt{2}]$. Moreover, when the right side of Eq. (25) attains its maxima of $\sqrt{2}$, the left side is 1, and when it attains its minima of $\sqrt{2}/2$, the left side is 0. Thus, the actual range should be smaller.

Since it is hard to analytically derive a tight bound from Eq. (25), we take a simulation approach to estimate a tighter one by generating a large number of random samples. Specifically, we first rewrite Eq. (22) and express $|s_i|$ as a function of ω_i:

$$|s_i| = \frac{1 \pm \omega_i \sqrt{2 - \omega_i^2}}{\alpha(\omega_i^2 - 1)} = \frac{\rho_i}{\alpha}, \tag{26}$$

where ρ_i is $\left(1 \pm \omega_i \sqrt{2 - \omega_i^2}\right)/\left(\omega_i^2 - 1\right)$ and the valid range of ω_i is $(1, \sqrt{2}]$. When ω_i is 1, s_i is undefined; AL cannot handle such a case; see Section 5.2. Accordingly, Eq. (25) can be written as

$$\frac{\alpha \sum_i |s_i|}{n} = \frac{\sum_i \omega_i \sum_i |s_i|}{n \sum_i \omega_i |s_i|} = \frac{\sum_i \omega_i \sum_i \rho_i}{n \sum_i \omega_i \rho_i}, \tag{27}$$

which is a function of $\{\omega_1, \cdots, \omega_n\}$. Since ω_i ranges $(1, \sqrt{2}]$, we randomly generate 10 millions test cases, where $n \in [10, 10^6]$, and obtain the range of Eq. (27) as $[0.81, 1.07]$. When the expression in Eq. (27) attains around 1.07, the input curves look like $y = \ln x$ with many small absolute slopes and several large ones. In Section 5.1, we show an experiment with a large collection of data, where the resulting average absolute slopes are mostly in [0.93, 1.0].

Lastly, note also that although we derive these bounds based on uniformly-sampled data points, the derivation is also applicable to non-uniformly sampled data, because we can include extra samples in a data set by interpolation to make it uniform.

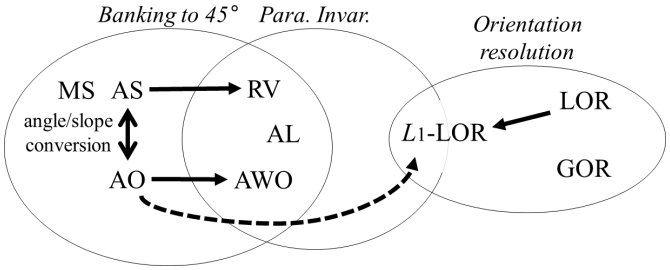

Fig. 6 Venn diagram to show the grouping relationship among various methods: banking to 45°, parameterization invariance, and orientation resolution. Moreover, we draw three kinds of arrows to show the connection relationships between individual methods: i) AS, AO and LOR are the parameterization variant forms of RV, AWO and L_1-LOR, respectively; ii) AS and AO are convertible between each other by angle and slope; and iii) AO has the potential to be similar to L_1-LOR.

4.2 Connecting RV and AS

Talbot et al. [9] showed that RV can be obtained by replacing the Euclidean distance with Manhattan distance to measure the arc length in AL. In this subsection, we provide another interpretation of RV, and show that it is a parameterization invariant form of AS. Such a result facilitates us to establish a connection between RV and the banking to 45° principle.

Again, we start with data points that are evenly spaced in x with a step size of Δx. Then, we can rewrite Eq. (4) as

$$\alpha = 1/\text{mean}|s_i| = \frac{n\Delta x}{\sum_i |s_i| \Delta x} = \frac{x_{n+1} - x_1}{\sum_i |s_i| \Delta x} = \frac{\sum_i |\Delta x_i|}{\sum_i |\Delta y_i|}, \tag{28}$$

where $\Delta x = (x_{n+1} - x_1)/n$ is a positive value. Hence, AS becomes equivalent to RV when the data points are evenly spaced in x. As shown in Fig. 3 (top row), AS produces the same plot (aspect ratio) as RV for the parameterization with $x = t$.

Compared with Eq. (10), we can see that Eq. (28) has the same formulation as RV, but is derived from a different background: extending AS using the line integral representation. Since AS is based on the banking to 45° principle, we say that RV also attempts to center the line segments around 45°. This relationship is also indicated by the boxplots shown in Fig. 9 , which summarize the average absolute slopes of different methods for all tested data sets shown in Fig. 7(a). We can see that RV produces the same average absolute slopes as AS.

4.3 Connecting L_1-LOR and AO

As reviewed in Section 2.3, the perceptual arguments of maximizing the orientation resolution and banking to 45° have been extensively used for choosing good aspect ratios. The equivalence between them was, however, discussed [7] only on simple cases with two line segments that have the same sign of slopes. Below, we provide new ways of exploring their equivalence, and show that methods built upon L_1-LOR and AO produce almost equivalent results for plots with multiple line segments.

If the orientations of every pair of successive line segments (i.e., θ_i and θ_{i+1}) have different signs, $|\theta_{i+1}-\theta_i| = |\theta_i|+|\theta_{i+1}|$, so we can rewrite Eq. (17) as

$$\begin{aligned}
&\max_{\alpha\in(0,\infty)} \sum_{i=1}^{n-1} \min(|\theta_i|+|\theta_{i+1}|, 180^\circ - (|\theta_i|+|\theta_{i+1}|)) \\
&= \min_{\alpha\in(0,\infty)} \sum_{i=1}^{n-1} \max(-|\theta_i|-|\theta_{i+1}|, |\theta_i|+|\theta_{i+1}|-180^\circ) + 90^\circ \\
&\qquad\qquad \text{(change outer min to max, and add } 90^\circ\text{)} \\
&= \min_{\alpha\in(0,\infty)} \sum_{i=1}^{n-1} \max[\, 45^\circ - (|\theta_i|+|\theta_{i+1}|)/2 \;,\; (|\theta_i|+|\theta_{i+1}|)/2 - 45^\circ \,] \;,
\end{aligned} \tag{29}$$

where $(|\theta_i|+|\theta_{i+1}|)/2$ is the midangle of two successive line segments. Eq. (29) shows that L_1-LOR aims to bank the midangle of all pairs of successive line segments to 45°. Its goal is more rigorous than AO, which considers only the average orientation. Hence, L_1-LOR and AO produce similar aspect ratios for plots with alternating orientation signs; see Figs. 5 (d,h) for examples.

From the signal processing point of view, successive line segments with alternating orientations are usually high frequency signals, unless the plot is fairly flat. Since data often contains high and low frequency fluctuations, L_1-LOR cannot be simplified to Eq. (29), but can perform more similar to AO for high frequency components. Fig. 5 illustrates this point by gradually adding white noise to the curve $y = 1/x$. Both L_1-LOR and AO select the same aspect ratio when the signal-to-noise ratio drops to 10.

4.4 Summary

Fig. 6 summarizes our findings with a Venn diagram to show various methods in groups, and arrows to reveal connection relationships between individual methods. By computing the bounds of the average absolute slope of AL, we show that AL tends to satisfy the banking to 45° principle (Section 4.1). In addition, we show that RV is the parameterization invariant form of AS, so RV inherently satisfies the banking to 45° principle (Section 4.2). Hence, in Fig. 6, we put AL and RV into the group of methods that banks to 45°, and draw the arrow from AS to RV. Furthermore, we build the connection between the two perceptual arguments (banks to 45° and maximizing the orientation resolution) by finding the condition that L_1-LOR performs similarly to AO. Hence, we draw the arrow with a dashed line from AO to L_1-LOR. Note also that L_1-LOR is partially inside the parameterization invariance group, since it has limited parameterization invariance.

5 Comparative Evaluation

We implemented all the aspect ratio selection methods listed in Table 1 in C++ and tested them on a PC with an Intel Core i5-4590 3.3GHz CPU and 8GB memory. We solve the optimization problems in AL, AO, AWO, L_1-LOR and LOR by the method-of-moving-asymptotes (MMA) [19], which is provided by the NLopt library [20]. Like Talbot et al. [9], we parameterize the optimization search with $\log(\alpha)$, so it converges faster than a direct search for α. To verify the conclusions derived in previous sections, we compare the aspect ratios selected by all existing methods on various data sets.

Data sets. Besides the data sets in Heer and Agrawala [7] and Talbot et al. [9], we downloaded more data from the UCI data set library [21], making it a total of 47 data sets of 1D curves; all of them have evenly spaced data points in x. Moreover, we followed Talbot et al. [9] and took 26 2D contour plots as inputs to try various methods in the same way as 1D curves. Note that 2D contours are generally non-uniformly sampled, so they are good candidates for investigating the parameterization invariance property. Nonetheless, if a 2D contours plot has strong physical meaning, e.g., a map, we do not modify its aspect ratio. All code and data sets are available for download on GitHub [1].

Measures. Since there are no metrics that quantify the effectiveness of an aspect ratio selection, we conduct comparisons by following Talbot et al. [9] to compute the log relative aspect ratio (in short, we call log-ratio). This ratio is defined as the logarithm of the relative ratio between the two α selected by the method being studied and a reference method, which is AL in [9]. Hence, a negative value means that the α selected by the method is smaller than the α selected by the reference; otherwise, the log-ratio is non-negative. Unlike Talbot et al. [9], we used RV as the reference because RV is parameterization invariant and easier to compute.

Results. Figs. 7 (a,b) present scatter plots of log-ratios generated by applying various methods to the 47 1D curves and 26 2D contours we collected, respectively. Due to space limitations, we show log-ratios only for some of the 1D curves; complete results can be found in the supplemental material. From the two figures, we can see that the ranges of the selected aspect ratios in the two scatter plots are very different. Most log-ratios in Fig. 7(a) are positive, while a few of them are much larger than zeros in Fig. 7(b). If a log-ratio value is out of the plot range, we treat it as an outlier and draw a dark transparent shadow in the plot to indicate their amount, where the plotted curve of 9-13 produced by AO shown in Fig. 8(e) provides one example. To facilitate the comparison among different methods, we summarize the resulting log-ratios associated with each method for each group of data sets (1D curves and 2D contours) in the two boxplots shown in Figs. 7 (c,d). We order the boxplots from left to right as follows: AL, the four methods based on average absolute slope/orientation (MS, AS, AWO and AO), and then the methods based on orientation resolution (L_1-LOR, LOR and GOR). For easy comparison, we put AL as the first column and RV as the last which is also the reference, and put L_1-LOR in-between AO and LOR, since it performs similarly to AO and relates to LOR.

Furthermore, it is worth to note that for LOR, AO and AS, a number of selected α are out of the (vertical) boxplot range; they are treated as the outliers. In the plots, we indicate these outliers using shadows whose size indicates the outlier amount. Moreover, for the case of AS, there are too many outliers, so part of the boxplot rectangle that represents the second and third quartiles is also out of the plot range. Lastly, for visual comparison, we show some 1D curves and 2D contours plotted with the aspect ratios selected by various methods in Fig. 8, where we follow the boxplot ordering, but put RV (reference) back. Complete results for plots over all different methods for all the data sets can be found in the supplemental material. By carefully inspecting them, we come up with the following four interesting observations:

- AL and AWO behave very similarly to RV for both 1D curves and 2D contours; their values of log(relative aspect ratios) are usually around zeros; see again Fig. 7(a);
- L_1-LOR behaves differently from RV but similarly to AO or LOR for some of the 1D curves; and

1. https://github.com/ArranWangzy/AspectRatioSelection

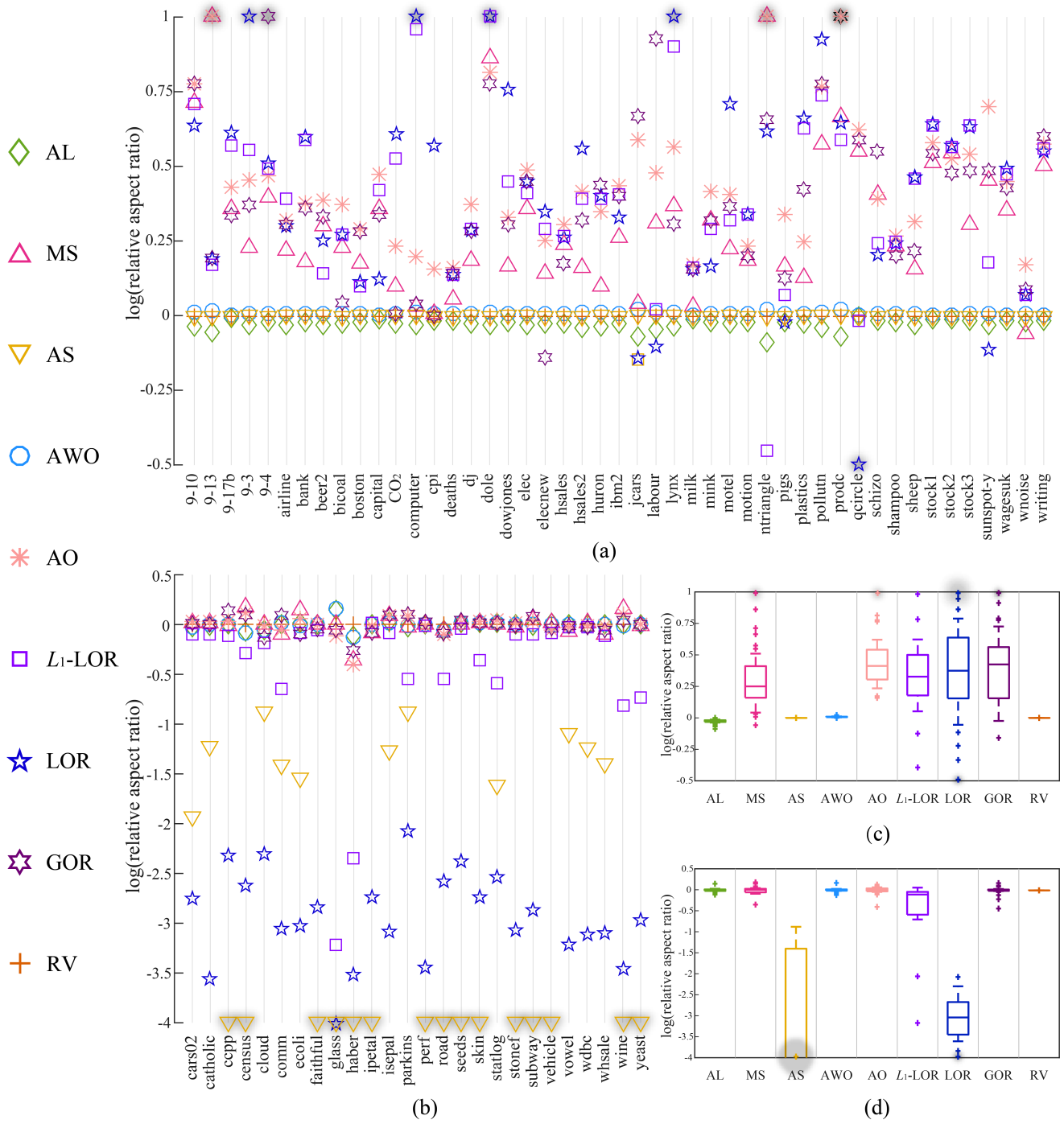

Fig. 7 Comparing the aspect ratios (presented as log relative aspect ratios, or log-ratios) produced by various methods on 1D curves (a) and 2D contours (b), relative to RV as the reference for computing the log-ratios. To reveal the distribution of log-ratios for each method, we summarize the log-ratios results shown (a) and (b) as boxplots in (c) and (d), respectively; in case a result is out of the plot range (see AS particularly), we draw a dark transparent shadow to indicate the outliers.

- for 2D contours, AS often selects much smaller aspect ratios, while AO and MS both behave similarly to RV.

Since some of these observations are inconsistent with the findings reported by Talbot et al. [9], this motivates us to further explore the underlying reasons behind the observations, to provide insights on which methods to be used for data with redundant samples, outliers, noise and non-uniform parameterization, and to discuss a common limitation of the existing methods. Before exploring the observations, we first verify if the average absolute slope generated by AL is around one.

5.1 AL and Banking to 45°

As discussed in Section 4.1, AS attempts to find an aspect ratio that yields an average absolute slope of one, whereas the bounds of the average absolute slopes for AL (i.e., [0.93,1]) slightly deviate from one. To explore whether the average absolute slopes for AL is around one, we computed the average absolute slopes for all the

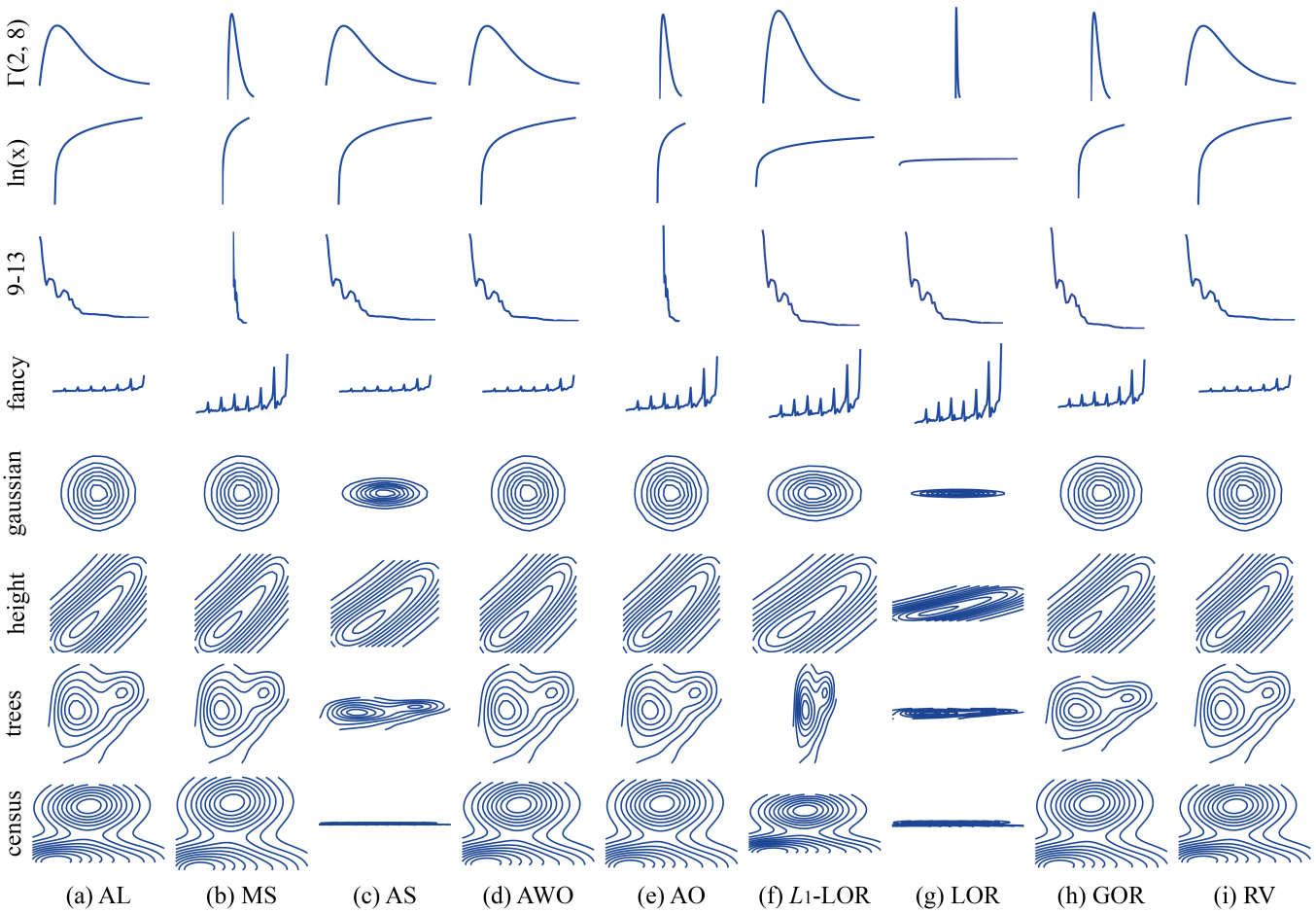

Fig. 8 We present the actual plots produced by using various methods on eight data sets: four (top) from Fig. 7(a) and four (bottom) from Fig. 7(b). Comparing these plots, we can see that RV, AL and AWO consistently produce almost the same plots for all the eight data sets, while L_1-LOR also produces reasonable plots but it behaves more differently from RV.

results behind Fig. 7, and summarized the average absolute slopes of all the methods for the 1D curve data sets in Fig. 9. For the case of AL, the average absolute slopes are roughly within [0.91,1.0], so AL selects aspect ratios similar to AS and tends to satisfy the banking to 45° principle. Note that our derivation in Section 4.1 assumes the data points to be equally spaced along x, so we do not compute the average absolute slopes for 2D contours, whose data are mostly non-uniformly sampled.

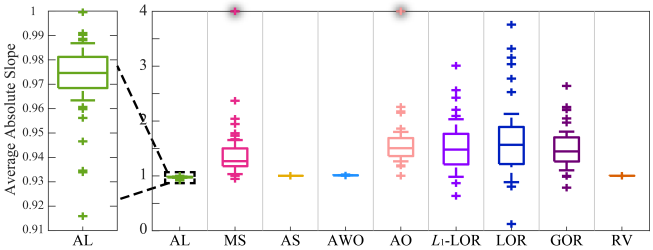

Fig. 9 These boxplots summarize the average absolute slopes (not log-ratios) for each method over all the 1D curve data set.

5.2 AWO vs. RV vs. AL

To verify whether AWO, RV and AL behave similarly, we extended the examples used by Talbot et al. [9]. Specifically, we synthesized a set of 1D gamma distributions (by setting the shape parameter as 2 and varying the scale parameter from 0.1 to 256) and 2D ellipses (by varying the major/minor axis ratio of an ellipse from 0.5 to 2). Then, we can explore how the parameters influence the aspect ratios selected by various methods.

Fig. 10 presents the relationships between the aspect ratios selected by the three methods and the associated varying parameters. It can be seen that AWO, RV and AL behave roughly the same for both data sets. All aspect ratios selected for the gamma distributions are close to 0.5 (Fig. 10(a)), while the aspect ratios selected for the ellipses consistently equal the associated major/minor axis ratios (Fig. 10(b)). This implies that AWO, RV and AL select almost the same aspect ratios for all the data sets. After discussing this result with the authors of AL [9], we think that their erroneous observation about the relation between AWO and AL is possibly due to an incorrect AWO implementation.

Data with redundant samples. Compared to AWO and AL, RV is faster and more stable due to its closed form. Looking at the aspect ratios shown in Fig. 10(a), RV can consistently produce an aspect ratio of 0.5, while results from AWO and AL have more fluctuations, due to the involved optimization processes.

For AWO and AL, gradient-based optimization is often used to solve for the aspect ratios. However, if the data has redundant samples, i.e., degenerated line segments with Δx_i=0 and Δy_i=0, the $\sqrt{\Delta x_i^2 + (\alpha \Delta y_i)^2}$ term in the derivatives of Eqs. (11) and (6) (see Appendix) will lead to zero denominators, and invalidate the

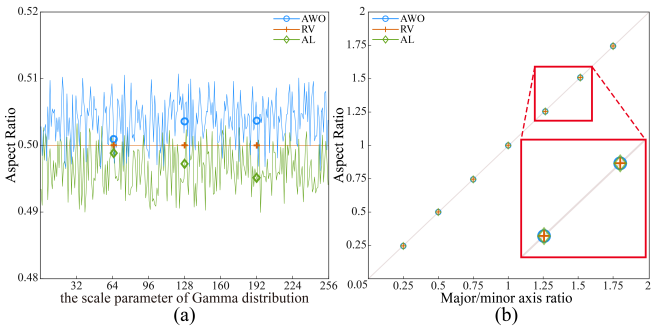

Fig. 10 Exploring how (a) changes in the scale parameter of the Gamma distribution and (b) major/minor axis ratio in ellipses influence the aspect ratios selected by AWO, AL and RV.

optimization. Hence, we have to filter out redundant data samples before applying gradient-based optimization, or use a derivative free optimization method [22]. In contrast, RV can address such an issue, so we suggest using RV as the default aspect ratio selection method. Moreover, note that AWO, AL and RV all degenerate when the input curve is a pure horizontal/vertical line, for which any nonzero aspect ratio is a reasonable result in practice.

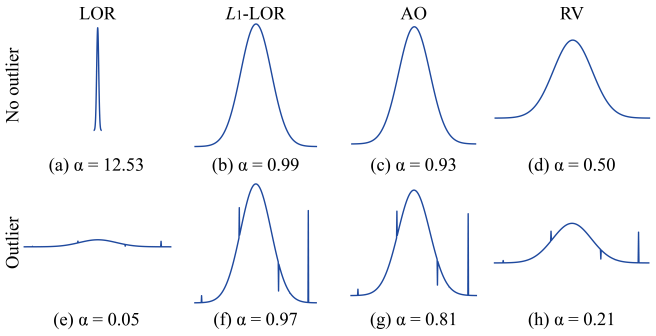

Fig. 11 Comparing the robustness of LOR, L_1-LOR, AO and RV on a *Gaussian* curve with (bottom) and without (top) outliers.

5.3 LOR vs. L_1-LOR vs. GOR vs. AO

Fig. 7 shows that LOR tends to select extremely large or small aspect ratios, whereas L_1-LOR and AO produce more reasonable ratios, especially for 2D contours. For 1D curves, LOR behaves similarly to L_1-LOR in most cases. We believe the reason is that the slopes are not too large (see data set *9-13* in Fig. 8 (3rd row)), so that the optimizations based on L_2 and L_1 norms produce similar results. For some data sets, e.g., *fancy* in Fig. 8, AO, L_1-LOR and LOR have similar behavior due to strong high frequency components in the curve. As discussed in previous works [7], [9], methods based on maximizing orientation resolution, including LOR, L_1-LOR and GOR, are not applicable to degenerated cases, where the resulting aspect ratio could be a random value. Compared to other methods, GOR involves a prohibitively expensive iterative optimization; thus, it is often not recommended [7].

Outlier. Although it is hard to find the global optimum for L_1-LOR, the L_1 norm in L_1-LOR makes it less sensitive, or more robust, to outliers in data [23], e.g., data points with extreme values compared to the neighbors. The reason is that L_1-LOR puts equal weights to all orientation resolutions, while LOR puts larger weight to large orientation resolutions by squaring the orientation

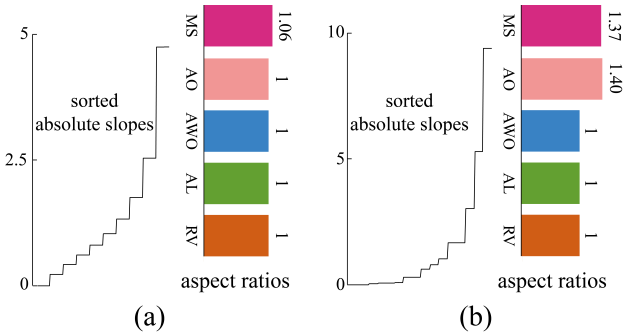

Fig. 12 Comparing the aspect ratios generated by MS, AO, AWO, RV and AL on 2D circular contours with (a) uniform and (b) non-uniform edge sampling, where the absolute slopes are sorted (from bottom to top in each plot) in the ascending order are shown on the left, whereas the selected aspect ratios are shown on the right.

resolution term. Hence, L_1-LOR can select similar aspect ratios for the same data with and without outliers; see Fig. 11, where LOR selects extreme aspect ratios.

Like L_1-LOR, both AO and RV compute aspect ratios by using L_1 norm, so their selected aspect ratios do not exhibit large variations as LOR; see again Fig. 11. However, AO may select extreme aspect ratios for some 1D curves as shown in Fig. 5(a), where the nearly horizontal line segments are squeezed in order to average the absolute orientation to 45°. Thus we do not suggest to use AO and LOR for practical usage.

In summary, we recommend L_1-LOR for inputs without degenerated line segments; otherwise, we should filter the data first.

5.4 AS, AO and MS

Fig. 7 shows that AS usually selects smaller aspect ratios than RV for contour plots, and behaves similarly to RV for 1D curves. This is because RV is the parameterization invariant form of AS.

Non-uniform Parameterization. AO and MS behave similarly to RV for most contour plots (see Fig. 7(b)), which is consistent with the observation of Talbot et al. [9]. However, it should be noted that AO and MS may not always select similar aspect ratios, e.g., see data set *census* in Fig. 7. To validate this observation, we synthesized a contour plot with 10 circles and then sampled the contours with 30 edges, both uniformly and non-uniformly. Results in Figs. 12 (a,b) show that AO and MS only behave similarly to RV for equally-sampled contours, while AWO, AL and RV always select exactly the same aspect ratio. The reason is that both AO and MS are *not* parameterization invariant.

Due to its simplicity, MS has been widely used in practice [5], [7]. Since the computation procedure of RV is even simpler than searching for the median and RV is parameterization invariant (thus more stable), we recommend to use RV instead of MS as the default aspect ratio selection method.

5.5 RV and L_1-LOR

Fig. 7 show that the aspect ratios selected by RV and L_1-LOR are similar for most 2D contours, and more different for all the 1D curves. However, L_1-LOR does not select extreme aspect ratios for most data, and the aspect ratios selected by the two methods could complement each other for all the 1D curves.

Noise. Since both RV and L_1-LOR use L_1 norm to compute the aspect ratio, they are robust to outliers as discussed in Section 5.3.

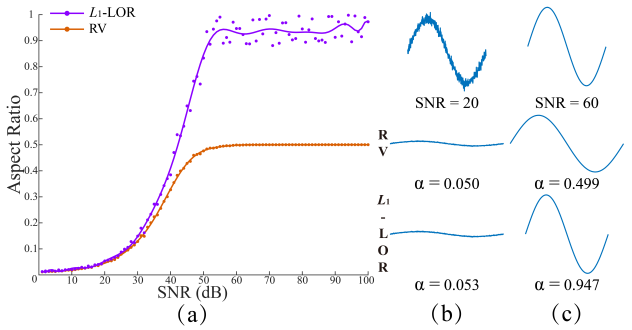

Fig. 13 Exploring the sensitivities of RV and L_1-LOR by adding white noise with varying SNR to the sin function. (a) The scatter plot and fitted curves show the relationship between the aspect ratios selected by L_1-LOR (pink) and RV (red) against SNR; (b,c) The input curves (top row, α=1) and curves plotted with the aspect ratios selected by RV (middle row) and L_1-LOR (bottom row).

We further study their sensitivities to noise by adding white noise with varying SNR to the sin function. Fig. 13(a) shows the relationship between the aspect ratios selected by RV and L_1-LOR against SNR. To compare the difference between the two methods, we fit two regression curves (pink and red) in Fig. 13(a), with which we can see that the aspect ratios selected by the two methods have large differences when the noise level is low (SNR>40). To explore the variations over different noise levels, we prepare two additional curves with SNR=20 and SNR=60 in Figs. 13 (b,c), respectively. We can see that both methods select too small aspect ratios when the noise level is large (see Fig. 13(b)), so that the trends in the data cannot be clearly presented. To address this issue, we suggest finding a suitable aspect ratio by using only the low frequency component in the data (see Section 6).

5.6 Summary

To support the goal of recommending methods for selecting aspect ratios in line charts, we summarize the behaviors of methods for 1D curves below:

- Although AL and AWO always perform similarly to RV, RV is faster and is the only method that can handle data with redundant samples;
- Compared to LOR and GOR, L_1-LOR is more robust and achieves certain parameterization invariance; and
- L_1-LOR and RV produce different aspect ratios for most data but performs similarly for the data with strong noise.

The first two findings above correspond to methods in the banking to 45° and orientation resolution groups, respectively; see the Venn diagram we constructed in Fig. 6. Taking the third finding into account, we suggest selecting aspect ratios by considering both RV and L_1-LOR; see Section 6 for more details.

A common limitation. It should be noted that neither RV nor L_1-LOR can choose reasonable aspect ratios for data with strong spike noise, i.e., data with very fast fluctuation in small scales; see the blue curve in Fig. 14(a). For such data, the average absolute orientation and the averaged orientation resolution are close to 90° and 0°, respectively; see Fig. 14(d). Note that for a data with n line segments, the average absolute orientation is defined as $\sum_i |\theta_i|/n$ (see Eq. (5) for the meaning of θ_i) and the averaged

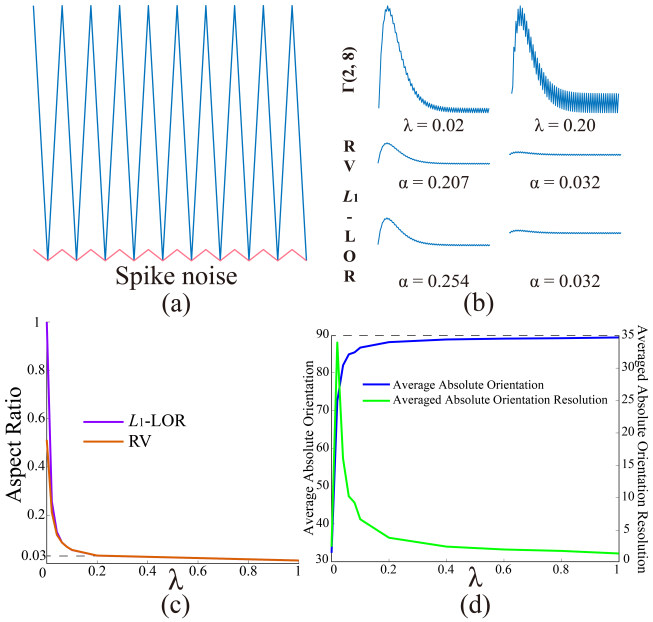

Fig. 14 Exploring the influence of spike noise on aspect ratios selected by RV and L_1-LOR. (a) The blue curve is the input spike noise and the pink one is plotted with the aspect ratio (0.04) selected by both methods; (b) adding varying amounts of spike noise (λ) to function $\Gamma(2,8)$ (top row) and the curves (middle & bottom rows) plotted with the aspect ratios selected by RV and L_1-LOR; and (c,d) the relationships between the aspect ratios selected by L_1-LOR and RV (c), the average absolute orientation (the blue curve in (d)), and the averaged absolute orientation resolution (the green curve in (e)) against λ (horizontal axis). These plots (c,d) show that when the amount of spike noise (λ) increases, the aspect ratios selected by both L_1-LOR and RV drop quickly, and the average absolute orientation quickly increases.

orientation resolution is defined as $\sum_{i=1}^{n-1} \gamma_{i,i+1}/n-1$ (see Eq. (7) for the meaning of γ). To bank data with strong spike noise to 45°, both RV and L_1-LOR have to choose an extremely small aspect ratio. For example, 0.04 is chosen as the aspect ratio for the blue curve in Fig. 14(a) to produce the pink curve.

We further study the influence of spike noise by adding varying amounts of spike noise (λ) to function $\Gamma(2,8)$; see Fig. 14(b). Fig. 14(c) shows the relationship between the aspect ratios selected by RV and L_1-LOR against λ. We can see that the aspect ratios quickly drop to around 0.03 when λ increases just to 0.2. Using extremely small aspect ratios, the resulting data plots would be flattened (see Fig. 14(b)), so the major data patterns are obscured. Hence, we suggest to apply a median filter to first smooth out the spike noise in the data before selecting the aspect ratio.

6 Dual-scale Banking

Essentially, RV and L_1-LOR reveal data trends in different scales, so we recommend to simultaneously use both of them to select aspect ratios, and refer the technique as the *dual-scale* banking.

6.1 Method

Given an input data set, dual-scale banking first considers if the data contains a large amount of spike noise; if this is the case, it will first apply a median filter [24] to smooth out the spike noise (see Section 5.6) before applying RV and L_1-LOR to compute two

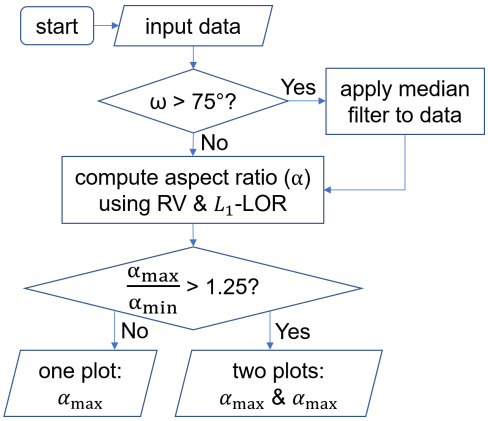

Fig. 15 Flowchart of dual-scale banking, where ω is the average absolute orientation of the input data, and α_{max} and α_{min} are the maximal and minimal aspect ratios selected by RV and L_1-LOR.

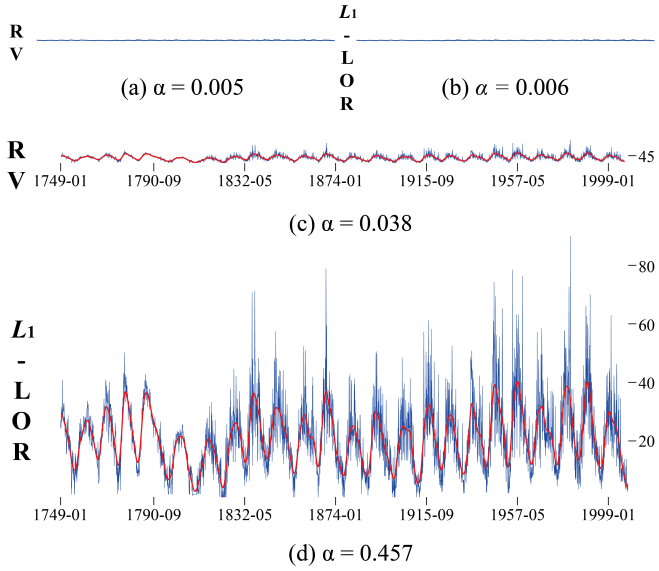

Fig. 16 Demonstrating the application of our dual-scale banking technique to the *Sunspot* data. (a,b) Plots produced by directly applying RV and L_1-LOR to the original data. The resulting aspect ratios are too small to reveal any meaningful patterns. (c,d) results of dual-scale banking, where we apply RV and L_1-LOR to a median-filtered curve (in red), and produce two plots (one by RV (c) and one by L_1-LOR (d)) to show complementary patterns.

aspect ratios on the data. Then, we check if the two ratios are close to each other. As suggested by Heer and Agrawala [7], if the ratio between the larger aspect ratio and the other one is less than 1.25, the two selected aspect ratios will reveal similar scales of interest; hence, we only use the larger aspect ratio to generate a single plot. Otherwise, we produce two plots with the two aspect ratios. Fig. 15 shows the flowchart of our dual-scaling banking method.

Dual-scale banking enables us to effectively reveal patterns of interest in different scales. As shown in Fig. 16, the filtered curve produced with RV can better show the oscillating period (see Fig. 16(c)) while the curve produced with L_1-LOR can better present the local maxima and their oscillations over the cycles (see Fig. 16(d)). However, dual-scale banking introduces a new task for the user to decide if the given data contains strong spike noise. As shown in Fig. 14(d), the average absolute orientation of the data quickly increases as λ increases to 0.1. Thus, we judge if the data requires median filter smoothing by checking whether the average absolute orientation of the data is larger than a given threshold. Through an experimental analysis, we set the threshold as 75°; see the supplemental material for details. Here, we do not use the averaged absolute orientation resolution because it is a second-order variable and is not as stable as the average absolute orientation; see Fig. 14(d).

6.2 Results

To demonstrate the applicability of our dual-scale banking technique, we apply it to a number of real-world data. Typically, we show results using the presentation style shown in Figs. 16 (c,d), where we overlay the computed trend curve (red) over the data (blue) plotted with the selected aspect ratio.

Dole. The first data set is *dole* [2], which is a classic example used by Talbot et al. [9] to illustrate the difference between AL and the other methods. This data set contains the number of persons receiving unemployment benefits in Australia from Jan. 1956 to Jul. 1992; note that the data is uniformly spaced over time. The aspect ratios and the resulting curves are presented in Fig. 1, where the aspect ratio selected by L_1-LOR is roughly three times larger than that of RV. We can see that Fig. 1(a) can better highlight the lower frequency trend in the data, while Fig. 1(b) can help to emphasize the higher frequency cycles of interest.

Sunspot Cycles. This time series [2] records the number and size of sunspots observed over a given period of time; note that sunspots are dark regions observed on the Sun. Here, we use the *sunspot* data set measured monthly from 1749 to 2008. From Figs. 16 (a,b), we can see that direct applications of RV and L_1-LOR to the raw input data would lead to too small aspect ratios, where interesting patterns are all annihilated. In such situation, dual-scale banking would apply RV and L_1-LOR to the curve after the median filter smoothing; see the red plots in Figs. 16 (c,d), and produce two new aspect ratios. As a result, we can present different patterns of interest and explore the same data in different perspective. For instance, Fig. 16(c) can better reveal the sunspot period, where each interval has a faster increase and more gradual decrease, while Fig. 16(d) can better reveal the local maxima and their fluctuations.

China Population. To demonstrate the advantage of being parameterization invariant for dual-scale banking, we apply it to the China population statistics data set [25] that ranges from BC 221 to 2010. Note that it was not possible to have uniform data over such a long period for various historical reasons, so the data is non-uniformly sampled. Fig. 17 shows the results, where the (unevenly distributed) marker points correspond to the existing numbers. Fig. 17(a) strongly emphasizes a significant increase in population that occurred since 1620 during the Qing Dynasty. In contrast, Fig. 17(b) reveals some oscillations before such increase, especially the one around 1063 during the Song dynasty.

In this example, most parameterization variant methods select larger or smaller aspect ratios, except AO. AO performs similarly to L_1-LOR (0.973 vs. 0.972), which is consistent with our analysis in Section 4.3. This result demonstrates that dual-scale banking can efficiently deal with non-uniformly sampled data.

7 Discussion And Future Work

In this paper, we present a comprehensive study on various kinds of aspect ratio selection methods by exploring their parameter-

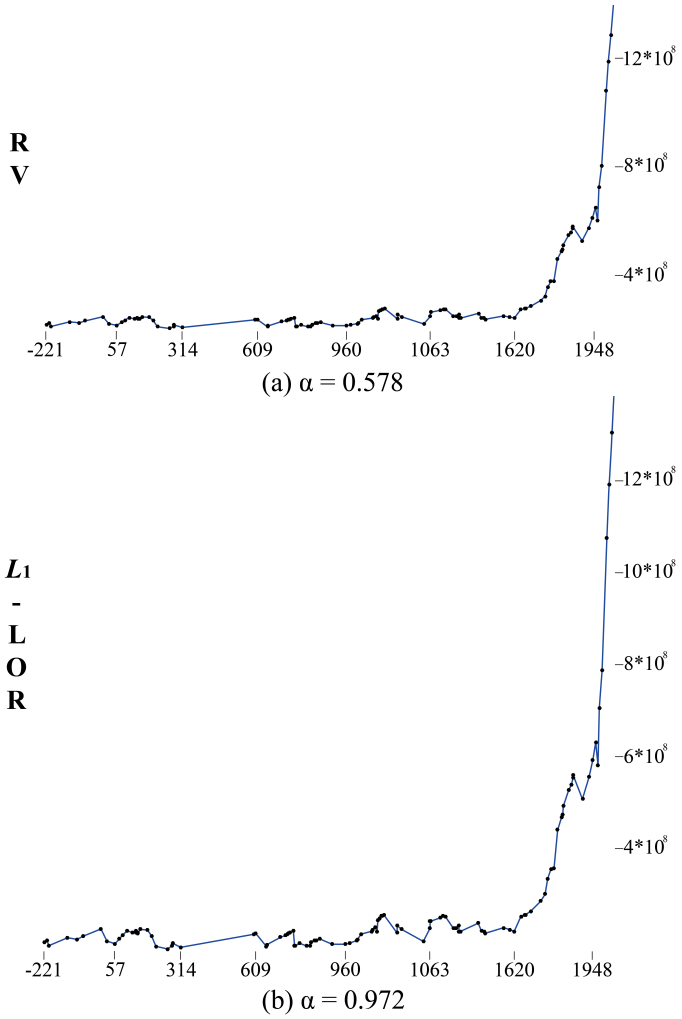

Fig. 17 Exploring the China population statistics using dual-scale banking. Two plots are produced with the aspect ratios selected by (a) RV and by (b) L_1-LOR, where (a) highlights the significant increase in population during the Qing dynasty (1636-1911), while (b) highlights other oscillations before the significant increase.

ization invariance, deriving their relationships, and conducting quantitative comparisons among them. The results lead to the following three guidelines for choosing aspect ratio selection methods: i), AL, AWO and RV always perform very similarly, but RV is faster and is the only method that can handle data with redundant samples; ii), L_1-LOR is more robust than LOR and GOR and has certain parameterization invariance; and iii) L_1-LOR produces reasonable but different aspect ratios compared to RV for most data. Based on these findings, we develop the dual-scale banking technique, aiming to take advantages of both RV and L_1-LOR when selecting aspect ratios and revealing data patterns. Lastly, we also demonstrate the effectiveness and parameterization invariance advantage of dual-scale banking on various real-world data sets.

Although we unveiled the parameterization invariance of most methods and mathematically derived the connections for several of them, there are still open questions about the mathematical foundation of various methods. First, we did not provide a formal proof to show that AL banks the line segments to 45°. Second, the differences among the aspect ratios selected by AL, AWO and RV were not explained. For most data, their aspect ratio values occur in the order AWO>RV>AL, while we observe AL>RV>AWO for a few algebraic curves such as $\ln(x)$. Lastly, we did not extensively investigate the condition for L_1-LOR and LOR to produce similar aspect ratios, although we know that their major difference is on the L_1 and L_2 norm in their formulations.

On the other hand, our quantitative comparison demonstrates that AWO, RL and RV perform similarly, while L_1-LOR produces results that are reasonable but different from RV's. The perceptual foundations of these methods are different. Both AWO and L_1-LOR are derived from the perceptual argument of maximizing the orientation resolution. Thus, we would like to investigate the equivalence between maximizing the orientation resolution and banking the line segments to 45° by studying how people judge the ratio of the slopes of multiple adjacent line segments. Regarding AL and RV, they lack adequate perceptual criteria, although the authors suggested some hypothesis [8], [9]. Investigating the visual cues to understand the perceptual justification of RV and AL is part of our ongoing work. Well-designed human subject evaluation will likely be necessary to learn whether the perceptual reasons behind all three methods are equivalent. In addition, extending RV and L_1-LOR to select suitable aspect ratios for line graphs with multiple time series [26] and 2D scatterplots [11] may provide more insights into their perceptual foundations.

APPENDIX

The derivative of Eq. (6) for AWO with respect to α is

$$\frac{1}{\sum_{i=1}^{n}\sqrt{\Delta x_i^2+\alpha^2\Delta y_i^2}}\sum_{i=1}^{n}\frac{\alpha\Delta x_i\Delta y_i}{\sqrt{\Delta x_i^2+\alpha^2\Delta y_i^2}},$$

while the derivative for Eq. (11) of AL is

$$\sum_{i=1}^{n}\frac{\Delta y_i^2-\frac{1}{\alpha^2}\Delta x_i^2}{2\sqrt{\frac{\Delta x_i^2}{\alpha}+\alpha\Delta y_i^2}}.$$

ACKNOWLEDGMENTS

The authors would like to thank the anonymous reviewers for the valuable comments. This work is supported by the grants of National Key Research & Development Plan of China (2016YFB1001404), NSFC (61772315), NSFC-Guangdong Joint Fund (U1501255), Science Challenge Project (No. TZ2016002), Shandong Provincial Natural Science Foundation (2016ZRE27617), and the Fundamental Research Funds of Shandong University. Yunhai Wang and Zeyu Wang are joint first authors, and Zhanglin Cheng is the corresponding author.

REFERENCES

[1] S. E. Palmer, *Vision science: Photons to phenomenology*. MIT press Cambridge, MA, 1999, vol. 1.
[2] R. Hyndman, "fma: Data sets from forecasting: methods and applications by makridakis, wheelwright & hyndman (1998)," *R package version*, vol. 2, 2009.
[3] W. S. Cleveland, M. E. McGill, and R. McGill, "The shape parameter of a two-variable graph," *Journal of the American Statistical Association*, vol. 83, no. 402, pp. 289–300, 1988.
[4] W. S. Cleveland, "A model for studying display methods of statistical graphics," *Journal of Computational and Graphical Statistics*, vol. 2, no. 4, pp. 323–343, 1993.
[5] ——, *Visualizing data*. Hobart Press, 1993.
[6] W. S. Cleveland *et al.*, *The elements of graphing data*. Wadsworth Advanced Books and Software Monterey, CA, 1994.
[7] J. Heer and M. Agrawala, "Multi-scale banking to 45°," *IEEE Trans. Vis. & Comp. Graphics*, vol. 12, no. 5, pp. 701–708, 2006.

[8] G. Saptarshi and W. S. Cleveland, "Perceptual, mathematical, and statistical properties of judging functional dependence on visual displays," Purdue University Department of Statistics, Tech. Rep., 2011.

[9] J. Talbot, J. Gerth, and P. Hanrahan, "Arc length-based aspect ratio selection," *IEEE Trans. Vis. & Comp. Graphics*, vol. 17, no. 12, pp. 2276–2282, 2011.

[10] F. Han, Y. Wang, J. Zhang, O. Deussen, and B. Chen, "Mathematical foundations of arc length-based aspect ratio selection," in *IEEE Pacific Visualization Symposium*, 2016, pp. 9–15.

[11] M. Fink, J.-H. Haunert, J. Spoerhase, and A. Wolff, "Selecting the aspect ratio of a scatter plot based on its delaunay triangulation," *IEEE Trans. Vis. & Comp. Graphics*, vol. 19, no. 12, pp. 2326–2335, 2013.

[12] J. Talbot, J. Gerth, and P. Hanrahan, "An empirical model of slope ratio comparisons," *IEEE Trans. Vis. & Comp. Graphics*, vol. 18, no. 12, pp. 2613–2620, 2012.

[13] C. Bennett, J. Ryall, L. Spalteholz, and A. Gooch, "The aesthetics of graph visualization." *Computational Aesthetics*, vol. 2007, pp. 57–64, 2007.

[14] J. Heer and M. Bostock, "Crowdsourcing graphical perception: using mechanical turk to assess visualization design," in *Proceedings of the SIGCHI Conference on Human Factors in Computing Systems*, 2010, pp. 203–212.

[15] N. Kong, J. Heer, and M. Agrawala, "Perceptual guidelines for creating rectangular treemaps," *IEEE Trans. Vis. & Comp. Graphics*, vol. 16, no. 6, pp. 990–998, 2010.

[16] L. Harrison, F. Yang, S. Franconeri, and R. Chang, "Ranking visualizations of correlation using Weber's law," *IEEE Trans. Vis. & Comp. Graphics*, vol. 20, no. 12, pp. 1943–1952, 2014.

[17] M. Kay and J. Heer, "Beyond Weber's law: A second look at ranking visualizations of correlation," *IEEE Trans. Vis. & Comp. Graphics*, vol. 22, no. 1, pp. 469–478, 2016.

[18] S. Tan, *Calculus: Early Transcendentals*. Cengage Learning, 2010.

[19] K. Svanberg, "A class of globally convergent optimization methods based on conservative convex separable approximations," *SIAM journal on optimization*, vol. 12, no. 2, pp. 555–573, 2002.

[20] S. G. Johnson, "The NLopt nonlinear-optimization package. 2011," *URL http://ab-initio.mit.edu/nlopt*.

[21] M. Lichman, "UCI machine learning repository," 2013. [Online]. Available: http://archive.ics.uci.edu/ml

[22] A. R. Conn, K. Scheinberg, and L. N. Vicente, *Introduction to derivative-free optimization*. SIAM, 2009.

[23] Y. Dodge, *Statistical data analysis based on the L1-norm and related methods*. Birkhäuser, 2012.

[24] R. Suoranta and K.-P. Estola, "Robust median filter with adaptive window length," in *IEEE International Symposium on Circuits and Systems*, 1991, pp. 108–111.

[25] J. Banister, "A brief history of China's population," in *The Population of Modern China*, 1992, pp. 51–57.

[26] W. Javed, B. McDonnel, and N. Elmqvist, "Graphical perception of multiple time series," *IEEE Trans. Vis. & Comp. Graphics*, vol. 16, no. 6, pp. 927–934, 2010.

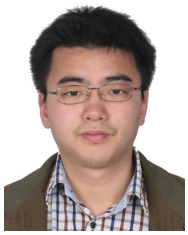

Yunhai Wang is an associate professor in School of Computer Science and Technology at Shandong University. He received his doctoral degree in computer science from Supercomputer center, Chinese Academy of Sciences, China in 2011. His interests include scientific visualization, information visualization and computer graphics.

Zeyu Wang is a third year undergraduate student in School of Computer Science and Technology at Shandong University. His research interests include visualization and computer graphics.

Lifeng Zhu is an associate Professor in the department of Instrument science and technology in Southeast University. He received his doctoral degree in computer science from Peking University in 2012. His research topics are visual computing and human computer interaction. His interests are in particular shape modeling and its applications in medical science and fabrication.

Jian Zhang received his Ph.D. degree in applied Mathematics from the University of Minnesota in 2005. After a postdoc at the Pennsylvania State University, he is now a research scientist in Supercomputing Center of Computer Network Information Center, Chinese Academy of Sciences (CAS). His current research interests include scientific computing and scientific visualization.

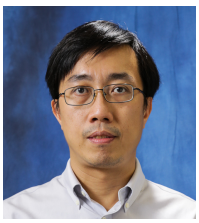

Chi-Wing Fu joined the Chinese University of Hong Kong as an associate professor from 2016. He obtained his PhD in Computer Science from Indiana University Bloomington, USA. He served as the program co-chair of SIGGRAPH ASIA 2016 technical brief and poster, associate editor of Computer Graphics Forum, and program committee members in various conferences including IEEE Visualization. His research interests include computer graphics, visualization, and user interaction.

Zhanglin Cheng is an associate Professor of Visual Computing Research Center in Shenzhen Institutes of Advanced Technology (SIAT), Chinese Academy of Sciences. He received the Ph.D. degree from Institute of Automation, Chinese Academy of Sciences in 2008. His research interests and experience span a wide range of topics including computer graphics, computer vision and visualization

Changhe Tu received the BSc, MEng, and PhD degrees from Shandong University, Jinan, P.R. China, in 1990, 1993, and 2003, respectively. His research interests are in the areas of computer graphics and visualization. He is a Professor in the School of Computer Science and Technology, Shandong University, China.

Baoquan Chen is now a Professor of School of Computer Science and Technology, Shandong University. He received his MS degree from Tsinghua University, Beijing, and PhD degree from the State University of New York at Stony Brook. He is the recipient of the NSF CAREER award 2003, IEEE Visualization Best Paper Award 2005, and NSFC Outstanding Young Researcher program in 2010. His research interests generally lie in computer graphics, visualization, and human-computer interaction.